Medical Freezers as Flexible Load for Demand Response in a Business Park Microgrid with Local Solar Power Generation

Rosa Morales González[1(✉)], Madeleine Gibescu[3], Sjef Cobben[1], Martijn Bongaerts[2], Marcel de Nes-Koedam[2], and Wouter Vermeiden[2]

[1] Eindhoven University of Technology, 5612AP Eindhoven, The Netherlands
{r.m.d.g.morales.gonzalez,j.f.g.cobben}@tue.nl
[2] Alliander NV, 6812AH Arnhem, The Netherlands
martijn.bongaerts@alliander.com, marcel.de.nes.koedam@qirion.nl, wouter.vermeiden@exe.energy
[3] Copernicus Institute for Sustainable Development, Utrecht University, 3584CB Utrecht, the Netherlands
m.gibescu@uu.nl

Abstract. This work presents a day-ahead demand response (DR) scheduling framework that quantifies the flexibility in non-residential buildings by using thermodynamic modeling, and assesses the benefits of DR in terms of three separate optimization variants: net payment minimization, energy self-sufficiency, and peak power reduction. We test the framework in a case study of a medical research facility located in a business park with local solar power generation. The flexible loads are four groups of independently-controlled medical freezers. Our DR framework generates optimal freezer operation and solar power production/curtailment schedules that are compared against a business-as-usual scenario with no DR. We perform simulations for cases with and without end-of-horizon temperature constraints. Results show that the flexibility harnessed from the freezers' thermal mass for DR actions improves the price-responsiveness, energy independence, and peak power consumption of the system with respect to the business-as-usual scenario. Furthermore, adding end-of-horizon constraints ensures that the thermal buffer of the flexible load will be full for the next simulation time window.

Keywords: Demand response · Genetic algorithm · Smart grid · Local RES integration · Physical systems modeling

1 Introduction

Smart grids, evolved from traditional power systems, propose innovative energy and operational measures to cope with present-day industry challenges, such as meeting sustainability targets, decarbonizing the energy supply, and dealing with aging infrastructure [1]. One such measure is to increase distributed generation from renewable

This work was supported by Alliander N.V.

B. Donnellan et al. (Eds.): SMARTGREENS 2018/VEHITS 2018, CCIS 992, pp. 23–43, 2019.
https://doi.org/10.1007/978-3-030-26633-2_2

energy sources (DG-RES) like solar and wind. However, these resources cannot be ramped up or down to adapt to the load profile, as is the case with fossil fuels in traditional power plants, thus adversely impacting the flexibility—i.e. the ability to adapt to changes in consumption or generation patterns—of the power system value chain.

In order to solve this problem, smart grid technologies also propose different solutions to make up for the lost flexibility on the generation side by harnessing flexible resources from other parts of the power system value chain. For example, by enhancing monitoring and control functionalities, adding electrical and/or thermal storage, creating novel electricity market designs, and increasing demand-side flexibility through demand response (DR) programs [2,3]. In this paper, we focus on the latter, and define demand response as the set of "actions voluntarily taken by consumers [and/or prosumers] to change their energy usage—either in terms of quantity or timing—in response to an external control signal" [4], e.g., price or a direct command from the aggregator or system operator.

Thermostatically controlled loads such as water heaters [5], refrigerators [6], and heating, ventilation and air conditioning (HVAC) systems [7] have been widely used as sources of demand-side flexibility in DR programs. Many authors have focused on harnessing the flexibility of residential consumers with not quite satisfactory results due to the following drawbacks, which are discussed in more detail in [8–11]: that individual loads have to be aggregated in large numbers, yet consumer engagement, participation and retention are low; and setup investments are high, yet funding and operational resources are lacking and/or dependent on subsidies.

On the other hand, focusing on commercial and industrial (C&I) consumers for DR seems like an interesting prospect because of the following advantages [12,13]:

- These types of consumer sites have higher consumption footprints and higher peak demands than residential consumers [14]
- Resource aggregation is facilitated by the physical proximity of similar types of loads, since C&I consumers are usually located in business parks/industrial sites.

The history of demand-side management strategies may have started with targeting industrial consumers [15], but the *ad hoc* strategies proposed in works that feature industrial loads such as [16–18], have been unable to create the basis for a systematic, more widespread implementation of DR in this consumer sector due to two main problems: industrial consumers' energy needs vary greatly from one another, and applications for DR can be restricted in scope due to the industrial processes used as flexible loads [19,20].

In the realm of commercial consumers, extensive discussions on the flexibility potential of office buildings' passive thermal capacitance and HVAC controls have been taken place in the public scientific discourse [21–24]. The positive findings on applying DR to commercial buildings are especially relevant in the Netherlands, where the service industry is the second largest energy consumer behind heavy industry [25], and is the economic sector with the highest added value and employment numbers in the Dutch economy [26]. In particular, the health services sector has been consistently ranked in the top three sectors of the Dutch economy [27].

With the above in mind, in this work we propose a multiphysics DR framework to evaluate the flexibility potential of a medical freezing warehouse located in a business park microgrid with local solar photovoltaic (PV) generation. In our DR frame-

work, freezer loads are shifted in time by automated actions scheduled on a day-ahead basis, controlling the medical freezers located at the consumer premises in four independent clusters, while treating the locally-available solar power generation as a curtailable resource.

We analyze the interactions between the thermal and electrical systems that make up our case study microgrid via an integrated, multiphysics simulation and optimization DR tool. Through this approach, we calculate the flexibility potential of the thermal mass of the freezer enclosure and contents in terms of energy shifted and/or saved. We also quantify the benefits in terms of energy self-sufficiency, price-responsiveness, and peak load reduction for the consumer, the local PV producer, and the operator of the business park microgrid. In order to test this framework, we designed two simulation experiments. In the first one, we make improvements to the practical implementation of our DR framework in MATLAB, with the hypothesis of improving computation times, by changing the way in which we optimize the design variables described in the problem formulation and comparing our results to those obtained in previous work [28]. The second simulation experiment was designed to add end-of-horizon temperature constraints to the original problem formulation. This was done in order to overcome a previous limitation of our model, in which the thermal inertia of the medical freezers was depleted at the end of the optimization horizon, requiring some recovery time during which DR could not be applied until the freezers could recharge their thermal buffers. The endpoint temperature constraints will limit the state of charge of the thermal buffer represented by the medical freezers.

The rest of the paper is organized as follows: Sect. 2 describes the methodology used; Sect. 3 describes the case study used for this work; Sect. 4 presents the results obtained from applying our DR framework to the case study; Sect. 5 discusses the results and the practical implications and limitations of our work; and, finally, Sect. 6 states the main conclusions of our work and gives a roadmap for future directions of the research.

2 Methodology

This section describes the mathematical models and algorithms that describe the optimization problems and physical systems that make up our DR framework.

2.1 Optimization Problem Formulation

Let the binary variable $\beta(i,t)$ signify the ON/OFF signal of the flexible thermostatic load of cluster i at time t. The net power imported from the grid of all I flexible loads, $P_{net}(t)$, after combining the predicted contribution of local DG-RES in the microgrid $P_{RES}(t)$ and the flexible load i at time t, $P(i,t)$, is expressed by (1):

$$P_{net}(t) = \sum_{i=1}^{I} \beta(i,t)P(i,t) - P_{RES}(t) \tag{1}$$

Our demand response optimization problem (2) will determine the flexible load operation $\beta(i,t)$ and PV production schedules $P_{RES}(t)$ over a given time horizon $t \in [t_o, t_f]$. The problem is constrained to:

– the safety temperature bounds $[T_{min}(i,t), T_{max}(i,t)]$ to which the flexible loads are subjected (2b);
– the physical constraints of local DG-RES production, $P_{RES}^{max}(t)$ (2c);
– the rated connection capacity, P_{max} (2d); and
– the state of charge of the thermal buffer by the end of the DR time window, $T_{ic}(i,t_f)$ (2e).

$$\min_{\beta, P_{RES}} \quad \Omega = \Phi \tag{2a}$$

$$\text{s.t.} \quad T_{min}(i,t) \leq T_{ic}(i,t) \leq T_{max}(i,t) \quad \forall i,t \tag{2b}$$

$$0 \leq P_{RES}(t) \leq P_{RES}^{max}(t) \quad \forall t \tag{2c}$$

$$|P_{net}| \leq P_{max} \tag{2d}$$

$$T_{ic}(i,t_f) = T_{min}(i,t_o) \forall i \tag{2e}$$

where Φ stands in for the three optimization variants that will be analyzed separately: minimizing energy exchanges with the regional grid Φ_e (3), peak power consumption Φ_p (4), and net energy payments Φ_c (8).

End-of-horizon temperature constraints (2e) are added to ensure that the thermal buffer will be replenished by the end of the optimization time window. This way, DR can be implemented again for the next time window without the need for recovery time, as was the case in [28].

The temperatures of the flexible thermostatic loads $T_{ic}(i,t)$ determine the overall available demand-side flexibility at any given time. T_{ic} and $P(i,t)$ are obtained from first-order dynamic models that will be discussed in Sect. 2.2.

$$\Phi = \Phi_e = \sum_{t=t_o}^{t_f} |E_{net}(t)| = \int_{t_f}^{t_o} |P_{net}(t)| dt \tag{3}$$

$$\Phi = \Phi_p = max(|P_{net}|) \tag{4}$$

For the net payment optimization problem, let $\lambda_{RES}(t)$ be the price the local consumer pays for buying locally-produced energy in the microgrid, $\lambda_{grid}(t)$ the price for buying electricity from the regional electricity supplier, and λ_{feedin} the tariff the local DG-RES producer gets for exporting energy to the regional distribution network (all in €/kWh). Let us assume that the DG-RES producer sells its electricity at a lower price than the consumer would pay for electricity from the regional electricity supplier, and that the feed-in tariff is considerably less than the monetary compensation it receives for selling electricity locally within the microgrid (5):

$$\lambda_{feedin} \ll \lambda_{RES}(t) < \lambda_{grid}(t) \quad \forall t \tag{5}$$

The consumer fees and revenue for the DG-RES producer are given in (6) and (7), respectively:

$$O_{cons} = \sum_{t=t_o}^{t_f} (\lambda_{RES}(t) E_{RES}(t) + \lambda_{grid}(t) E_{imports}(t)) \tag{6}$$

$$O_{prod} = \sum_{t=t_o}^{t_f} (\lambda_{RES}(t) E_{RES}(t) + \lambda_{feedin}(t) E_{exports}(t)) \tag{7}$$

where $E_x(t) = \int_{t-1}^{t} P_x dt$, and x is a stand-in for subscripts *imports*, *exports*, and *RES*. $E_{imports}$ represents energy consumed from grid imports in the microgrid (i.e., when $E_{net} > 0$) at time t, and $E_{exports}$ signifies the locally produced energy from DG-RES fed back into the grid (i.e., when $E_{net} > 0$). Maximizing producer revenue and minimizing consumer fees, we have that the net payment is:

$$\Phi = \Phi_c = \sum_{t=1}^{T} (\lambda_{grid}(t) E_{imports}(t) - \lambda_{feedin}(t) E_{exports}(t)) \tag{8}$$

2.2 Thermostatic Load Modeling

This section describes the thermostatic load modeling approach used to obtain the inputs for the optimization problem described in Sect. 2.1.

Thermostatic load behavior can be described by a first-order dynamic system, as detailed in works such as [29–31]. Said first-order system can also be represented schematically as a lumped parameter resistor/capacitor (RC) circuit model, as shown in Fig. 1, to understand how the thermal mass of buildings determine the available demand-side flexibility in terms of shifting power and duration. The main advantages of this modeling approach are:

- its capability of capturing first-order transients of the flexible loads with a reasonable degree of accuracy without the need for a heavily-detailed simulation;
- it can facilitate the real-time implementation of the optimization framework we use in our DR program, since the modeling effort and computation time are considerably less than those required to create and simulate a more sophisticated model.
- it integrates the thermal and electrical domains, for a multiphysics, multidisciplinary analysis of the energy usage of flexible thermostatic loads.

The system of equations describing the temperature evolution over time of the different components of the flexible thermostatic loads is given in (9):

$$(mc_p)_{ic} \frac{dT_{ic}(t)}{dt} = -\frac{T_{ic}(t) - T_{in}(t)}{R_{ic-in}} \tag{9a}$$

$$(mc_p)_{in} \frac{dT_{in}(t)}{dt} = \frac{T_{ic}(t) - T_{in}(t)}{R_{ic-in}} - \frac{T_{in}(t) - T_{sup}}{R_{in-sup}} - \sum_{n=1}^{N} \frac{T_{in}(t) - T_{e,n}(t)}{R_{e,n,1} + R_{e,n,2}} \tag{9b}$$

$$(mc_p)_{e,n} \frac{dT_{e,n}(t)}{dt} = \frac{T_{in}(t) - T_{e,n}(t)}{R_{e,n,1} + R_{e,n,2}} - \frac{T_{e,n}(t) - T_{amb}(t)}{R_{e,n,3} + R_{e,n,4}} \quad \forall n \in [1, N] \tag{9c}$$

$$0 = \frac{T_{in}(t) - T_{sup}}{R_{conv}} + \beta(t) \dot{Q}_{sup}(t) \tag{9d}$$

where $(mc_p)_x$ denotes heat capacity in J/K; $dT_x(t)/dt$, is the rate of change temperature with respect to time in K/s; and R_x signifies thermal resistance in K/W. The subscript x is a stand-in for the subscripts ic, in, sup and e, n, (see corresponding blocks

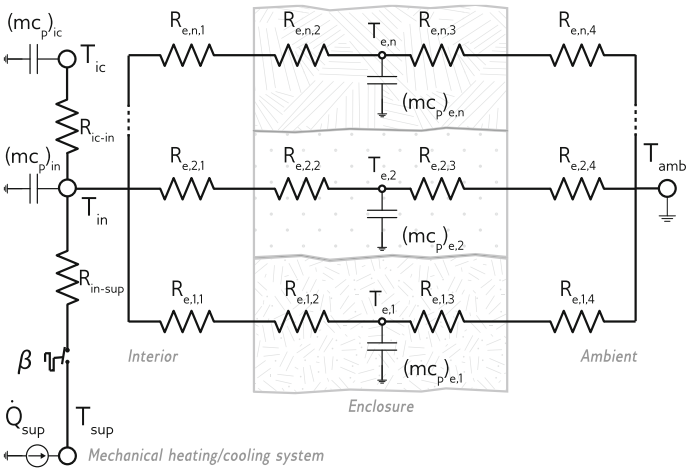

Fig. 1. Equivalent RC circuit of a flexible thermostatic load *(Adapted from* [28]*)*.

in Fig. 1) which describe the flexible thermostatic load, indoor air, mechanical heating/cooling/refrigeration supply system, and n number of enclosure elements out of a total N (e.g., roof, walls, floor), respectively. $T_{amb}(t)$ is the temperature of the ambient or conditioned space in which the flexible thermostatic loads are kept as a function of time in degrees Kelvin, $\dot{Q}_{sup}(t)$ is the heat extracted or added by mechanical cooling/heating system in watts, and T_{sup} is the supply temperature of the mechanical heating/cooling/refrigeration system in K.

The coefficient of performance (COP) determines the proportionality between mechanical heat added/extracted to the system and electrical power consumption of the thermostatic load $\dot{W}_{el}(t)$ (10):

$$COP(t) = \dot{Q}_{sup}(t)/\dot{W}_{el}(t) \tag{10}$$

The assumption of a constant COP is reasonable when the conditioned space in which the flexible thermostatic loads are kept is maintained at a constant temperature to ensure an optimal operation. In that case, mechanical heat extracted is given by (11):

$$\dot{Q}_{sup}(t) = COP \times \dot{W}_{el}(t) \tag{11}$$

Assuming we can independently control the operation of the flexible loads in i groups, as discussed in the previous section, we can substitute Eq. (2d) with (12):

$$P_{net}(t) = \sum_{i=1}^{I} \beta(i,t)\dot{W}_{el}(i,t) - P_{RES}(t) \tag{12}$$

2.3 Model Interactions and Implementation of the DR Framework

Because we have both continuous and discrete decision variables and the constraints are nonlinear, finding the optimality conditions to solve our problem through tradi-

tional mathematical methods can be time-consuming and cumbersome [32]. We therefore need to employ iterative heuristic search techniques to solve our mixed-integer nonlinear optimization problem in order to keep the computation time within reason.

In previous work, $\beta(i,t)$ and $P_{RES}(t)$ were optimized simultaneously (see Fig. 2(a) [28]. In practice, the software implementation of the problem in MATLAB turned out to be quite costly in terms of the computation time and resources to find the optimality conditions for both sets of variables due to the limitations inherent to the software. Therefore, in this work, we propose to optimize $\beta(i,t)$ and $P_{RES}(t)$ separately (Fig. 2(b) in two sub-optimization routines, with the hypothesis that this will decrease the computation time and improve results. In principle, this decoupling might lead to suboptimal results. In order to mitigate this effect, however, we set $P_{RES}(t) = P_{RES}^{max}(t)$ in the thermostatic load sub-optimization routine to take full advantage of locally available DG-RES production, and then run the second sub-optimization routine to trigger DG-RES curtailment actions when necessary. The inputs and outputs of the proposed DR framework are shown in Fig. 3, which also shows the sequential optimization of the operation schedules of the thermostatic loads and DG-RES production.

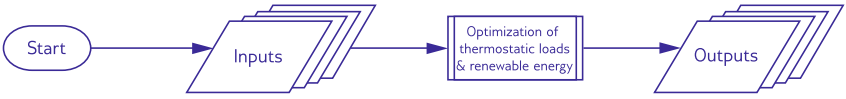

(a) Simultaneous optimization of all design variables schedules.

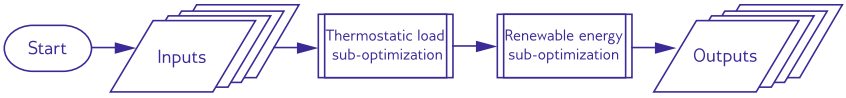

(b) Separate sub-optimization routines for each design variable.

Fig. 2. Demand response flowcharts.

As can be observed from the figure, our multiphysics DR framework consists of a cyclical interfacing of thermostatic load models with an optimization framework to: (1) calculate the available demand-side flexibility from the inherent thermal mass of the thermostatic loads; and (2) to devise optimal operation strategies for the flexible loads, such that the objectives of minimal net payment, maximal energy self-sufficiency or minimum peak load are achieved on a day-ahead basis. This means that the operation and PV production schedules are determined for the entire time horizon in advance of real-time, assuming perfect knowledge of wholesale and local day-ahead market prices, feed-in tariffs, as well as accurate forecasts of PV production.

3 Case Study

This section describes the case study and simulation experiments.

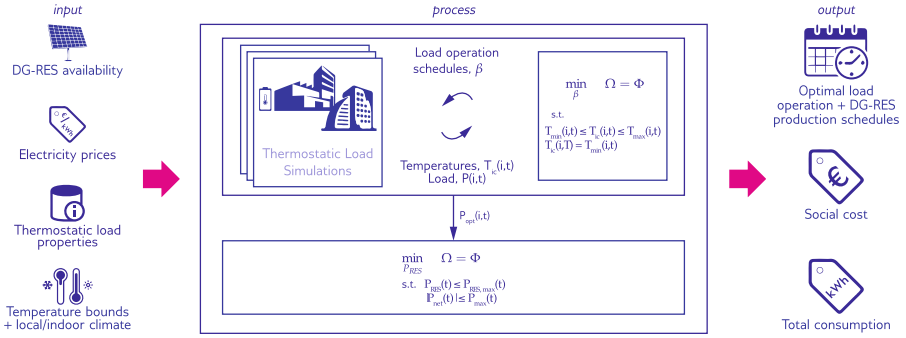

Fig. 3. Model interactions in the proposed DR framework *(Adapted from* [4]*)*.

We test our proposed DR framework in a case study of a medical research facility in the Netherlands, which is located in a business park with a 250-kWp photovoltaic installation (1700 m^2 of crystalline PV panels with a 12% system efficiency). The administrators of the medical research facility would like to implement demand response in order better utilize locally-available PV generation and reduce their electricity consumption fees.

The annual electricity consumption at the research facility is 1.4 GWh/y, of which approximately 35% of the load (500 MWh/y) is due to 120 freezer units of 1.1 kW each. When the freezers are all ON simultaneously, the peak load is 132 kW. The freezers are utilized for the long-term storage (in the order of years) of blood samples preserved in a high-concentration glycerol solution at -80 °C, and will be used as our flexible thermostatic load for the case study.

3.1 Model Inputs

This section describes the inputs used for the MATLAB/Simulink thermostatic load models.

Best practices in cryogenic preservation of biomaterials require glycerolized blood samples to be stored continuously at $-65\,°C$ or colder. The samples can be subjected to temperature variations without detriment under the aforementioned conditions [33]. We set the flexibility temperature thresholds for the internal contents of the medical freezers to a conservative range: $T_{ic} \in [-80, -70]°C$. A tolerance of $\pm 0.3\,°C$ is added to account for system delay.

The ultra-low-temperature freezers used in the medical research facility are kept at a constant ambient temperature of 25 °C. The COP at this temperature is 0.575, per manufacturer data. The physical properties of the enclosure materials and conditioned air inside the enclosure are listed in Table 1.

The amount of flexibility gained from the blood samples is given by:

$$Q_{flex} = (\rho V c_p)_{samples} \Delta T \tag{13}$$

where ρ and c_p are physical properties of the glycerolized blood samples, given in Table 1; $\Delta T = T_{max} - T_{min}$; and V is the total volume of the samples, which is 57.6 L

Table 1. Physical properties used to model the thermostatic loads.

Component	Density ρ [kg/m^3]	Specific heat capacity c_p [J/(kgK)]	Thermal conductivity k [W/(mK)]
Blood samples [33–35]	1063	1500	0.26
Air [36]	1	1000	0.02
Freezer enclosure [37,38]	186	650	0.01

when the freezer stores 1-ml samples and is at its full volumetric capacity. Substituting values in (13), we obtain that the total flexibility gained from the blood samples in the 120 freezers is $Q_{flex} = 30.61$ kWh per discharge cycle.

3.2 Assumptions

The assumptions made for the case study are enumerated below:

1. The heat transfer mechanisms considered for the thermostatic load modeling are conduction and convection. Radiation is deemed negligible due to the low emissivity values of the freezer enclosure materials and the high convective and conductive heat transfer rates from the air distribution system and evaporator coils in the freezers' interior.
2. Because the blood samples are kept in long-term storage, we assume that:
   (a) the internal contents of the freezer are already "at temperature"; i.e., the mechanical refrigeration system will only be used to maintain the product temperature; and
   (b) there is no in- or outflow of samples during the entirety of the DR time window.
3. Base electricity loads, loads triggered by human interaction (e.g. lighting), and heating/cooling loads required to balance ventilation and internal heat gains/losses within the medical research facility are neglected, since they are all considered inflexible loads.
4. Day-ahead electricity prices for the consumer and DG-RES producer (λ_{grid}, λ_{RES}), as well as the DG-RES feed-in tariffs (λ_{feedin}) are known.
5. PV generation can be forecasted with a reasonable degree of accuracy.

Expected day-ahead electricity prices[1] and PV generation values for typical irradiation days[2] used in the simulations are shown in Figs. 4 and 5.

3.3 Simulation Scenarios

We consider two simulation experiments for our DR program, in which we separately test three optimization variants:

– reduction of energy imports and exports from- and to the regional grid (3),

[1] Based on data from https://transparency.entsoe.eu/.
[2] Based on data from http://www.soda-pro.com/web-services#radiation.

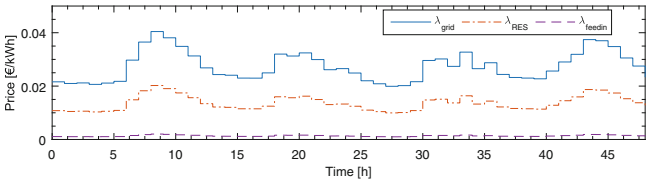

Fig. 4. Dynamic electricity prices for the end-users of the microgrid [28].

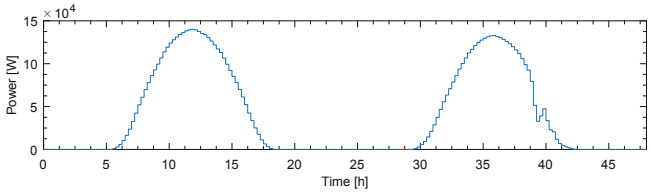

Fig. 5. PV production profiles for two consecutive average solar irradiation days in the Netherlands ($1700m^2$, system efficiency 12%) [28].

– net payment minimization (8), and
– peak load reduction (4).

In the first simulation experiment, we replicate the conditions of [28]: 48-h simulation window, 15-min resolution, no end-of-horizon temperature targets. Instead of optimizing our design variables $\beta(t)$ (772 elements) and $P_{RES}(t)$ (193 elements) simultaneously (966 design variables in total), we perform two separate sub-optimizations: one in which we solve for $\beta(t)$ with $P_{RES}(t) = P_{RES}^{max}(t)$, and a second one where we use the outputs of the first ($P_{opt}(t)$ in Fig. 3) to optimize $P_{RES}(t)$.

In the second simulation experiment, we apply end-of-horizon temperature constraints (2e) to see the effect of limiting the state of charge of the thermal buffer for all three optimization variants. We compare the results of these optimizations against a business-as-usual (BAU) scenario, where all freezers are operated as a single unit (worst-case scenario for peak load), and whose temperature controls consist of continuously-operating thermostats with a fixed setpoint and deadband based on the interior chamber temperature T_{in}. In this experiment, $\beta(t)$ has 388 elements and P_{RES} has 97 elements. In this scenario, we also optimize our design variables in separate sub-optimization routines as described in Sect. 2.3.

In both simulation exercises, we set P_{max} to the worst-case scenario for peak load, or 132 kW, in constraint (2d), and control our flexible load in four independent clusters of 30 freezers.

Simulations of our DR framework were carried out in MATLAB/Simulink using a double-processor Intel Xeon CPU with 28 cores and a clock speed of 2.6 GHz. The heuristic we chose for solving the optimization problem was the genetic algorithm (GA) as implemented by the MATLAB Optimization Toolbox, for its ability to deal with both continuous and discrete variables. We parallelized the search of feasibility conditions of the problem into 28 computational threads with the Parallel Computing Toolbox.

Because of the nature of the optimization problem and the iterative solution method we chose for it, it is not possible for us to obtain a global optimum. Instead, we found a number of local minima in successive simulation runs and selected the best ones to report in the next section.

4 Results

This section presents the simulation results for the two case studies detailed in Sect. 3.3.

4.1 Comparison Between Simultaneous and Separate Optimization of Design Variables

Figures 6, 7, 8 show the simulation results of the DR program when $\beta(t)$ and $P_{RES}(t)$ are optimized separately, for each of the optimization variants: energy, net payment and peak reduction, respectively. Each figure contains three subplots that are a function of time: (a) plots the temperature of the interior contents of each cluster of independently controllable freezers; (b) indicates how many groups of freezers are switched ON; and (c) graphs the electrical power consumption of the flexible load and the generation of the PV system, with positive values denoting consumption and negative values denoting generation.

In Fig. 6 we see that exchanges with the grid are kept as close to zero as possible during the day, when solar power generation is available (7:00–18:00 and 31:00–41:00 h),

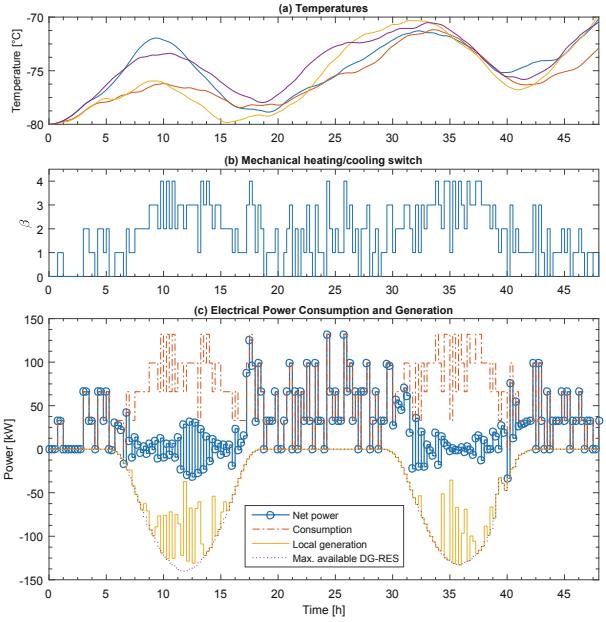

Fig. 6. Energy optimization with $\beta(t)$ and $P_{RES}(t)$ optimized separately.

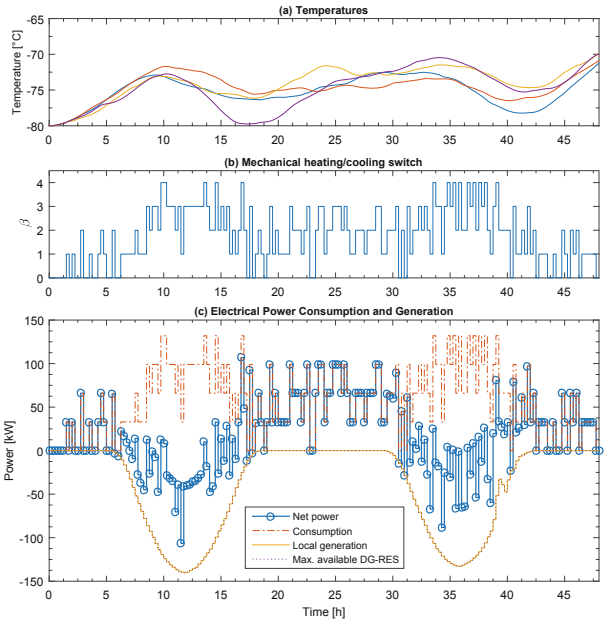

Fig. 7. Cost optimization with $\beta(t)$ and $P_{RES}(t)$ optimized separately.

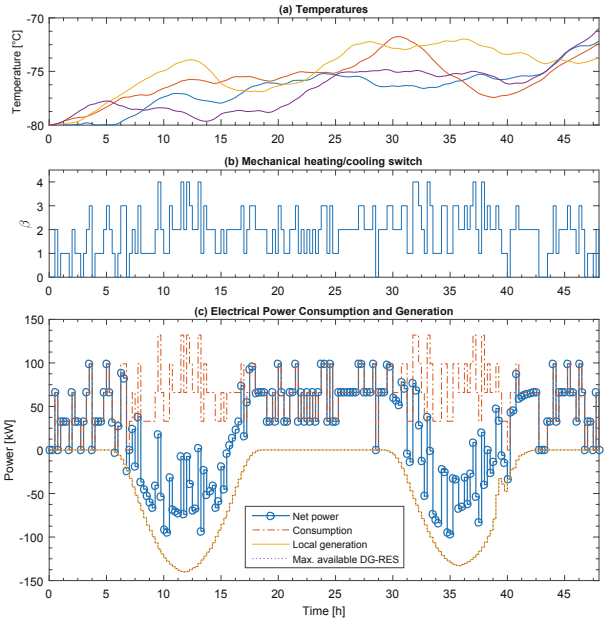

Fig. 8. Peak minimization with $\beta(t)$ and $P_{RES}(t)$ optimized separately.

and that, during the evening and early morning, the temperatures of the interior contents of the freezer are allowed to drift toward the upper bound by switching ON as few clusters of freezers as possible. In this scenario, we observe that PV generation is curtailed at several points during the day in order to keep the energy exchanges with the grid to a minimum, which comes at a detriment to the PV producer.

In Fig. 7 it is possible to observe that the flexible thermostatic loads are switched ON not only at the times where solar power is available, but also at the times when the electricity prices are low (approximately from 0:00–6:00, 15:00–19:00, 24:00–30:00 and 37:00–43:00 h). The general temperature trend during those hours is descending. In this scenario, PV production is fully utilized, thus maximizing the profit for the PV producer.

In Fig. 8, the peak power minimization objective is apparent: only three freezer clusters are ON simultaneously during the periods when there is no PV production. During daylight hours, all freezer clusters can be ON, since PV production offsets the load peak. In this scenario, PV production is also fully utilized.

Table 2 compares the results obtained by optimizing $\beta(t)$ and $P_{RES}(t)$ separately against those obtained by optimizing $\beta(t)$ and $P_{RES}(t)$ in a single genotype. The table shows the best and median values for the objective function evaluations, the computation times, and the PV utilization ratios from the successive simulation runs we performed for each scenario. From the figures and table, we can conclude that the results are comparable with one another, with the following notable improvements achieved by the sequential optimization of $\beta(t)$ and $P_{RES}(t)$:

- PV utilization rates increased.
- Better local minima were achieved in a slightly shorter amount of time.

The results confirm our hypothesis that optimizing our decision variables separately would decrease the computation time. We attribute this improvement to (1) a smaller search space due to the reduced number of variables, and (2) limiting the genotypes in the GA to either discrete or continuous elements instead of combining both types of variables in a single solution vector. The improved results obtained are attributable to an increased PV utilization rate, resulting from optimizing β assuming maximum PV production over the entire time horizon and then curtailing P_{RES} in the second suboptimization routine whenever necessary (see Fig. 2b).

4.2 Simulation Results Using Endpoint Constraints

This section presents and discussed the results obtained from the simulation experiments that included temperature end-of-horizon constraints (2e) in order to limit the state of charge of the freezers' thermal buffer, determined by Q_{flex} (13) and the heat loss rate through the the freezer enclosure elements (9c).

Table 3 shows the results for the three optimization variants with endpoint constraints, compared against the BAU scenario. In the table, the column entitled "Total exchange" is the sum of imports and exports from- and to the regional distribution grid. Figure 9 shows simulation results for the BAU scenario. This figure is analogous to Figs. 6, 7, 8, with the exception that subplot (a) shows the temperature evolution over time of the freezer contents (blue solid line) and indoor air temperatures

Table 2. Optimization results comparison.

	Objective function evaluation			Computation time [h:mm]		PV Utilization [%]	
Optimization variant	Best	Median	Unit	Best	Median	Best	Median
β and P_{RES} optimized simultaneously (from [28])							
Energy	1.52	1.77	MWh	1:22	1:34	77	64
Cost	36.92	42.69	€	1:21	1:46	88	87
Peak load	99	105.7	kW	1:11	1:20	53	49
β and P_{RES} optimized separately							
Energy	1.24	1.25	MWh	1:11	1:13	98	85
Cost	31.71	35.05	€	1:11	1:13	100	100
Peak load	99	103.0	kW	0:58	0:58	100	100

Table 3. Optimization results with endpoint constraints vs BAU scenario.

	Energy [kWh]			[€]	Reduction [%]			
Optimization variant	Consumption	Production	Total exchange	Net payment	Cost	Energy	Peak	PV utilization
BAU, no DR	1699.5	1006.7	1616.5	29.80	–	–	–	100
Energy	1489.1	666.42	840.5	22.45	25	48	5	66
Cost	1534.5	1006.7	1118.3	21.73	27	31	5	100
Peak load	1546.9	971.65	1154.01	22.76	24	29	29	97

(red solid line). Figures 10, 11, 12 graphically depict the simulation results for the energy, net payment and peak power minimization optimization variants for the endpoint constraints experiment.

In the BAU scenario, we can see that the uncontrolled infeed of power generated by the PV modules increases the peak from 132 kW (the peak output of the freezers) to 140 kW, because there is no consumption at the time when PV generation is highest (12:00 h). In the three optimization variants we can observe how the thermal buffer starts to deplete, but by around midday, the DR algorithm forces the freezers to start cooling again so that by the end of the horizon the temperature will be the same as the starting temperature $-80\,^{\circ}$C, and thus the thermal buffer will be full again. Because of the large time constant of the system and the relatively short simulation time horizon, we see that the temperatures never reach the upper bound of $-70\,^{\circ}$C. From this, we can conclude that adding endpoint constraints reduces the amount of flexibility available for DR actions, but eliminates the need for the system to recover (i.e., recharge its thermal buffers) after the DR time window has passed.

When comparing the results of this section to those obtained in Sect. 4.1, despite observing a difference in temperature evolutions brought about by the endpoint constraints (subplot a in Figs. 10, 11, 12), similar power consumption/generation trends can be observed for each optimization variant (subplot c in Figs. 10, 11, 12). In other words:

– The net energy exchanges with the electricity grid are reduced in the energy minimization scenario during times of solar energy production.

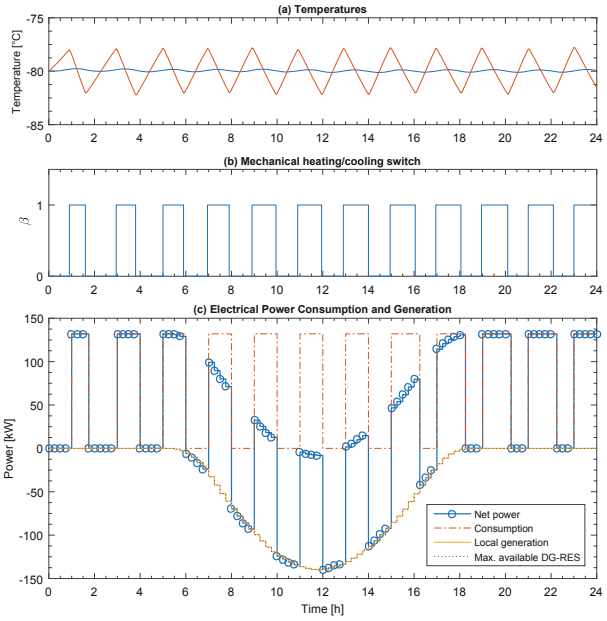

Fig. 9. BAU scenario 24-h.

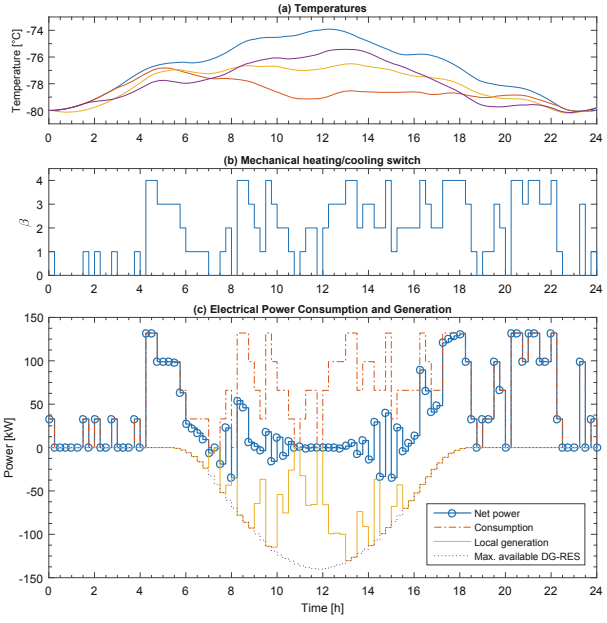

Fig. 10. Energy optimization with end-of-horizon temperature target.

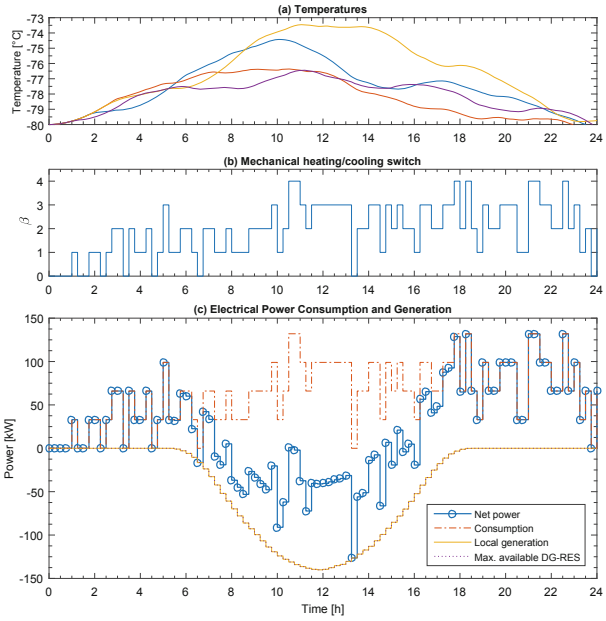

Fig. 11. Cost optimization with end-of-horizon temperature target.

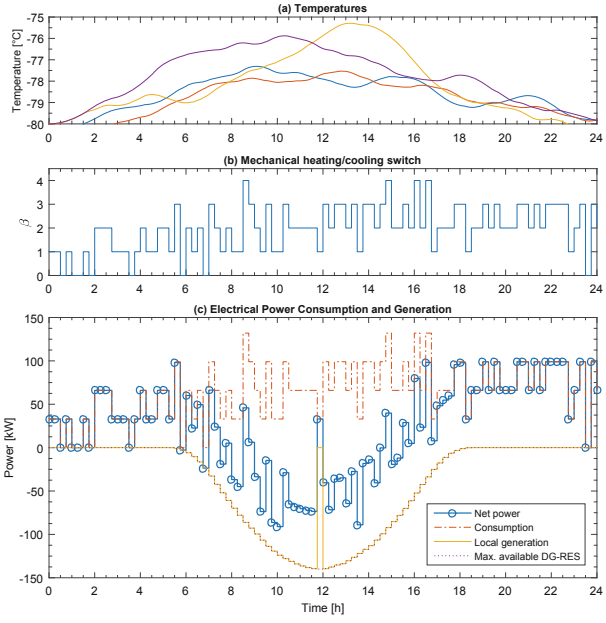

Fig. 12. Peak minimization with end-of-horizon temperature target.

– The periods of cheap electricity prices and solar energy production are taken advantage of in the net payment minimization scenario.
– The freezer clusters are operated three-at-a-time during periods of no solar power production, and are only allowed simultaneous operation during daylight hours.
– peak power is kept at less than or equal to the rated maximum power selected for these experiments in all three optimization variants.

The difference in electricity consumption between the results obtained when applying DR and the BAU scenario in Table 3 gives the total amount of flexibility gained from the freezers over the 24-h time horizon: 210 kWh for the energy minimization, 165 kWh for the net payment minimization, and 153 kWh for the peak load reduction objectives.

5 Discussion

This section further discusses the results obtained in the previous section and touches upon some limitations regarding the practical implementation of the proposed DR framework.

Results from the first simulation experiment confirm our initial hypothesis that optimizing the decision variables in separate, yet sequential optimization sub-problems would result in shorter computation times (22–30% less time) using the GA solver as implemented in MATLAB. We also achieved improvements in local minima and PV utilization rates by assuming maximum PV production for the thermostatic load scheduling sub-optimization routine and only curtailing DG-RES after obtaining an optimal load schedule. By reducing the number and type of variables for each sub-problem, the search spaces become smaller, and it takes a smaller number of generations to achieve the same or a better solution than solving the full optimization problem. However, it must be noted that separating the optimization problem into two (potentially suboptimal) subroutines is merely a compromise between achieving reasonable computation times and finding better local minima, given the chosen implementation in software of our DR framework. It would be worth investigating the effects of this using more powerful solvers.

The results from both Sects. 4.1 and 4.2 show the potential of implementing both price-responsive (net payment minimization) and direct control (peak load minimization) DR programs to harness flexibility from C&I customers' thermostatic loads. The employment of flexible loads brings about clear and attractive benefits in terms of reductions in the amount and overall electricity demand payments for consumers. Apart from the consumer benefits, the peak load reduction objective can also be beneficial for the network operator: the peak load reduction by 29% with respect to the BAU scenario with uncontrolled infeed of solar power could translate into deferrals in network reinforcement investments and/or lower connection fees.

Although the energy minimization case does not quite fall under the definition of DR programs, it still is an interesting variant to look at in terms of energy self-sufficiency for the consumer. However, the greater energy efficiency, while being in the interest of the microgrid as a whole, comes at a loss for the local PV producer due to occasional PV curtailment.

A possible expansion of our framework would be to combine all optimization variants into a single problem formulation by adding utilization constraints linked to the investment or operation expenses for the PV producer, and include peak capacity tariffs in the objective function.

Surmounting some of the assumptions made when computing the optimal schedules, especially with regards to dealing with errors in the PV forecasting data, will take additional effort before this DR framework can be rolled out into the field. In addition, although we have achieved shorter convergence times than in previous works, we need to take further steps to decrease the computation in order to move from the DR simulation environment into the the actual customer site. This issue can be resolved by using a more powerful commercial solver than those offered by the MATLAB Optimization Toolbox. Another possibility is to keep using MATLAB, but add a heuristic within the GA solver to filter out infeasible solutions based on heuristic calculations of the charging- and discharging rates of the system's thermal buffer, thus eliminating the need to perform the time-costly thermostatic load simulations in Simulink. A compromise between the quality of the solutions and the computational effort will be required when we scale up our DR framework to include more flexible sources in a business park.

6 Conclusions

This work presented a DR framework that schedules thermostatic loads and DG-RES production in advance of real-time (24–48 h) by using thermostatic load modeling techniques and a nonlinear optimization problem in order to quantify and deploy the demand-side flexibility in non-residential, C&I buildings. We assessed the benefits of DR in a series of case studies with and without end-of-horizon temperature constraints, where the flexible loads were 120 medical freezers containing blood samples, located in a research facility in a business park with local solar power generation.

Results show that the thermal buffer created by the thermal mass of the freezers' contents can be harnessed by automated DR actions to improve the price-responsiveness, energy independence and peak load of the system with respect to the business-as-usual scenario, by reducing load coincidence, improving consumer energy fees and equipment performance; and mitigating peak loads due to uncontrolled infeed of DG-RES that could allow the grid operator to defer investments in network reinforcements. Adding endpoint constraints reduces the amount of flexibility available for DR actions with respect to the scenario with no endpoint constraints, but eliminates the need for the system to recover (i.e., recharge its thermal buffers, represented by the medical freezers) immediately after the DR time window has passed.

Future work will extend the scope of our proposed DR framework to include the business park microgrid network constraints, and will add new flexibility sources in the business park, such as other building systems, thermal buffers (e.g. stratified hot water tanks), and/or electric vehicles.

Glossary

BAU Business-as-usual

C&I Commercial and industrial

COP Coefficient of performance

DG-RES Distributed generation from renewable energy sources

DR Demand response

GA Genetic algorithm

HVAC Heating, ventilation and air conditioning

PV Photovoltaic

RC Resistor/capacitor

References

1. Hewicker, C., Hogan, M., Mogren, A.: Power Perspectives 2030: on the road to a decarbonised power sector. Technical report, Roadmap 2050, Den Haag (2012)
2. Huber, M., Dimkova, D., Hamacher, T.: Integration of wind and solar power in Europe: assessment of flexibility requirements. Energy **69**, 236–246 (2014)
3. Alizadeh, M.I., Parsa Moghaddam, M., Amjady, N., Siano, P., Sheikh-El-Eslami, M.K.: Flexibility in future power systems with high renewable penetration: a review (2016)
4. Morales González, R., Shariat Torbaghan, S., Gibescu, M., Cobben, S.: Harnessing the flexibility of thermostatic loads in microgrids with solar power generation. Energies **9**, 547 (2016)
5. Gelažanskas, L., Gamage, K.A.A.: Distributed energy storage using residential hot water heaters. Energies **9**, 127 (2016)
6. Liu, W., Wu, Q., Wen, F., Ostergaard, J.: Day-ahead congestion management in distribution systems through household demand response and distribution congestion prices. Smart Grid, IEEE Trans. **5**, 2739–2747 (2014)
7. Yoon, J.H., Baldick, R., Novoselac, A.: Dynamic demand response controller based on real-time retail price for residential buildings. IEEE Trans. Smart Grid **5**, 121–129 (2014)
8. He, X., Keyaerts, N., Azevedo, I., Meeus, L., Hancher, L., Glachant, J.M.: How to engage consumers in demand response: a contract perspective. Util. Policy **27**, 108–122 (2013)
9. Klaassen, E., Frunt, J., Slootweg, J.: Method for evaluating smart grid concepts and pilots. In: IEEE Young Researcher Symposium 2014 (YRS 2014), Ghent, pp. 1–6. EESA (2014)
10. Dhulst, R., Labeeuw, W., Beusen, B., Claessens, S., Deconinck, G., Vanthournout, K.: Demand response flexibility and flexibility potential of residential smart appliances: experiences from large pilot test in Belgium. Appl. Energy **155**, 79–90 (2015)
11. Labeeuw, W., Stragier, J., Deconinck, G.: Potential of active demand reduction with residential wet appliances: a case study for Belgium. IEEE Trans. Smart Grid **6**, 315–323 (2015)

12. Ashok, S., Banerjee, R.: Load-management applications for the industrial sector. Appl. Energy **66**, 105–111 (2000)
13. Grünewald, P., Torriti, J.: Demand response from the non-domestic sector: early UK experiences and future opportunities. Energy Policy **61**, 423–429 (2013)
14. European Environment Agency: Final energy consumption by sector and fuel (2017)
15. Lampropoulos, I., Kling, W.L., Ribeiro, P.F., van den Berg, J.: History of demand side management and classification of demand response control schemes. IEEE Power Energy Soc. Gen. Meet. **2013**, 1–5 (2013)
16. Matthews, B., Craig, I.: Demand side management of a run-of-mine ore milling circuit. Control Eng. Pract. **21**, 759–768 (2013)
17. Mitra, S., Sun, L., Grossmann, I.E.: Optimal scheduling of industrial combined heat and power plants under time-sensitive electricity prices. Energy **54**, 194–211 (2013)
18. Finn, P., Fitzpatrick, C.: Demand side management of industrial electricity consumption: promoting the use of renewable energy through real-time pricing. Appl. Energy **113**, 11–21 (2014)
19. Samad, T., Kiliccote, S.: Smart grid technologies and applications for the industrial sector. Comput. Chem. Eng. **47**, 76–84 (2012)
20. Ton, D., Smith, M.: The U.S. department of energy's microgrid initiative. Electr. J. **25**, 84–94 (2012)
21. Zavala, V.M.: Real-time optimization strategies for building systems. Ind. Eng. Chem. Res. **52**, 3137–3150 (2013)
22. Ma, K., Hu, G., Spanos, C.J.: A cooperative demand response scheme using punishment mechanism and application to industrial refrigerated warehouses. IEEE Trans. Ind. Inform. **11**, 1520–1531 (2015)
23. Yin, R., et al.: Quantifying flexibility of commercial and residential loads for demand response using setpoint changes. Appl. Energy **177**, 149–164 (2016)
24. Hurtado, L.A., Mocanu, E., Nguyen, P.H., Gibescu, M., Kamphuis, I.G.: Enabling cooperative behavior for building demand response based on extended joint action learning. IEEE Trans. Ind. Inform **14**(1), 127–136 (2017)
25. Centraal Bureau voor de Statistiek: Energieverbruik; opbouw, bedrijfstak (2017)
26. Compendium voor de Leefomgeving: Bruto toegevoegde waarde en werkgelegenheid 1995–2016 (2017)
27. Centraal Bureau voor de Statistiek: Monitor topsectoren 2017 (2017)
28. Morales González, R., Gibescu, M., Cobben, J., Bongaerts, M., de Nes-Koedam, M., Vermeiden, W.: Demand response of medical freezers in a business park microgrid. In: SmartGreens 2015–7th International Conference Smart Cities Green ICT System, Funchal, SciTePress, pp. 1–10 (2018)
29. Kalsi, K., Chassin, F., Chassin, D.: Aggregated modeling of thermostatic loads in demand response: a systems and control perspective. In: 2011 50th IEEE Conference Decision Control European Control Conference (CDC-ECC), Orlando, pp. 15–20. IEEE (2011)
30. Hurtado, L., Mocanu, E., Nguyen, P., Kling, W.: Comfort-constrained demand flexibility management for building aggregations using a decentralized approach. In: 2015–4th International Conference Smart Cities Green ICT System SmartGreens, Lisbon, pp. 157–166 (2015)
31. Wilson, M.B., Luck, R., Mago, P.J.: A first-order study of reduced energy consumption via increased thermal capacitance with thermal storage management in a micro-building. Energies **8**, 12266–12282 (2015)
32. Sioshansi, R., Conejo, A.J.: Optimization in Engineering: Models and Algorithms. Springer, Cham (2017). https://doi.org/10.1007/978-3-319-56769-3
33. Eftekhar, J.G.: Some thermophysical properties of blood components and coolants for D5U. Technical report, University of Texas San Antonio, San Antonio (1989)

34. Wessling, F., Blackshear, P.: The thermal properties of human blood during the freezing process. Heat Transf. **95**, 246–249 (1973)
35. Zhang, A., Cheng, S., He, L., Luo, D., Gao, D.: Determination of thermal conductivity of cryoprotectant solutions and cell suspensions. Cell Preserv. Technol. **2**, 1–6 (2004)
36. Shpilrain, E.E.: AIR (PROPERTIES OF) (2011)
37. ASM Aerospace Specification Metals Inc.: (AISI Type 304 Stainless Steel)
38. MatWeb: Unifrax Excelfrax 200 VIP Vacuum Insulation Panel (2017)